Journal of Sound and Vibration (2001) **246**(1), 1–28
doi:10.1006/jsvi.2000.3116, available online at http://www.idealibrary.com on IDEAL®

PASSIVE VIBRATION CONTROL OF AIRBORNE EQUIPMENT USING A CIRCULAR STEEL RING

J. Ellison and G. Ahmadi

Department of Mechanical and Aeronautical Engineering, Clarkson University, Potsdam, NY 13699-5725, *U.S.A.*

and

M. Kehoe

NASA Dryden Flight Research Facility, Edwards, CA 93523, *U.S.A.*

(*Received* 12 *April* 1999, *and in final form* 10 *May* 2000)

Vibration isolation is needed to protect avionics equipment from adverse aircraft vibration environments. Passive isolation is the simplest means to achieve this goal. The system used here consists of a circular steel ring with a lump mass on top and exposed to base excitation. Sinusoidal and filtered zero-mean Gaussian white noise are used to excite the structure and the acceleration response spectra at the top of the ring are computed. An experiment is performed to identify the natural frequencies and modal damping of the circular ring. Comparison is made between the analytical and experimental results and good agreement is observed. The ring response is also evaluated with a concentrated mass attached to the top of the ring. The effectiveness of the ring in isolating the equipment from base excitation is studied. The acceleration response spectra of a single-degree-of-freedom (s.d.o.f.) system attached to the top of the ring are evaluated and the results are compared with those exposed directly to the base excitation. It is shown that a properly designed ring could effectively protect the avionics from possible damaging excitation levels.

1. INTRODUCTION

Vibration control technology is used in many applications in order to protect equipment, structures or mechanisms from undesirable vibration environments. The isolator design is normally based on the degree of isolation desired and the frequency range of the disturbance. Munjal [1] has organized vibration isolators into groups according to their functions and Snowdon [2] described the use and function of various isolators. Vibration isolation technology has been used in automobiles, aircraft, spacecraft and even buildings. Applications in the automobile are geared primarily toward improving ride quality. Aircraft design uses range from power plant, frictional damping of gas turbine blades [3] and active engine mounts [4] to flutter suppression [5]. Agnes *et al.* [6] described the vibration problems and solutions typical of fighter aircraft. Space applications vary in scope from structural control such as demonstrated by the INFLEX experiment [7] to microgravity isolation [8]. Recently, application of vibration isolation to the Space Shuttle was studied by Lee-Glauser *et al.* [9] and the Space Station vibration control was discussed by Ellison *et al.* [10]. In the area of earthquake engineering, frictional base isolation systems have been developed to protect large buildings [11–13].

0022-460X/01/360001 + 28 $35.00/0

Equipment mounted in aircraft are exposed to a varied vibration environment depending on the location of the installation and flight condition as illustrated by Dreher [14]. A survey of environmental data measured in flight such as vibration, acoustic, shock, thermal, flutter and loads was compiled by Hain *et al.* [15] to define a "real-world" aircraft environment. One particular example is detailed in the vibration and acoustic measurements report on the F-111A aircraft [16]. The vibration environment directly influences the operation, performance and life expectancy of airborne equipment. To that end, test techniques were developed to evaluate the avionics equipment endurance based on the source of vibration, installation and response of the black box [17].

In order to reduce the environment at the equipment, use of vibration isolation has been suggested. A number of passive and active vibration control techniques are available and the choice depends on the degree of isolation that is desired or necessary [18–21]. Typical passive isolators consist of a resilient element contained in a metallic-supporting frame. Generally, the resilient element is an elastomer, air, steel spring, wire rope or metal mesh [22]. Wire rope isolators are highly effective in controlling both shock and vibration [23]. Passive isolators are usually capable of up to 80 per cent isolation if the isolator natural frequency is less than one-fourth of the lowest excitation frequency. Tuning of the isolator may be necessary to achieve such high levels of isolation [24]. Active control is used when additional protection is needed.

In this work, a passive isolation system is studied as a prelude to a combined active/passive system for protecting an avionics box subjected to base excitation. The base isolation system is composed of stainless-steel circular rings placed on the base corners of the avionics box. This system has the capability of isolating the equipment in various directions. In this initial study, the avionics box is modelled as a lumped mass and only a single ring isolation system is considered. The earliest work performed on the free vibration of a circular ring was reported by Hoppe [25]. Further work expanding the scope of the ring vibration problem considered centerline extension [26] and shear deformation and rotary inertia [27–30]. In most of the earlier works, the general ring vibration properties were analyzed but no particular vibration isolation applications were studied. Here, the ring is treated as a component of a passive isolation system and its performance in protecting the equipment against the adverse vibration environment is evaluated.

An experiment is also conducted to evaluate the vibration characteristics of a typical circular steel ring for comparison with the analysis. The experiment consisted of a circular steel ring mounted on top of a small electrodynamic shaker with the response measured by an accelerometer. The test is performed with and without an attached mass on top of the ring. These data are then used to verify the computational model.

Sinusoidal and random base excitations are considered and the peak responses of the ring and attached single-degree-of-freedom (s.d.o.f.) systems are evaluated. It is shown that the ring could effectively reduce the peak acceleration transmitted to the avionics equipment.

2. MODEL FORMULATION

Passive base isolation of an avionics box with the use of circular, stainless-steel ring supports attached to each corner of the equipment is shown schematically in Figure 1. In this study, however, we are concerned with the in-plane motion of a single ring. We also assume that the avionics box behaves as is a rigid mass. The basic configuration of this model, which consists of a thin stainless-steel ring rigidly attached to a base structure and a concentrated mass located at the top, is shown in Figure 2.

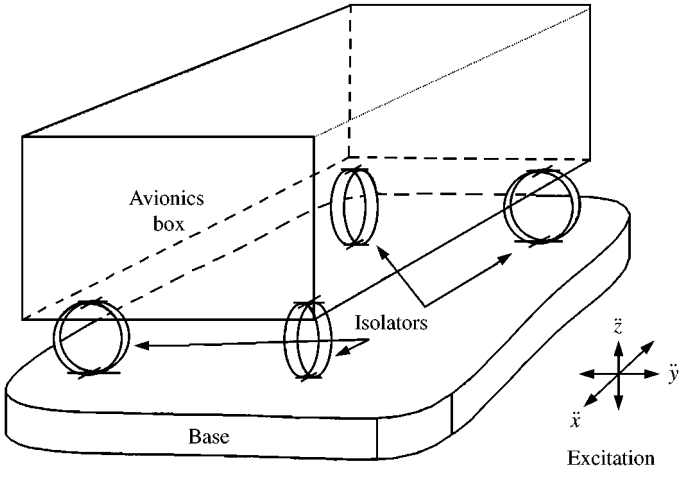

Figure 1. Circular ring isolation system for generic avionics equipment.

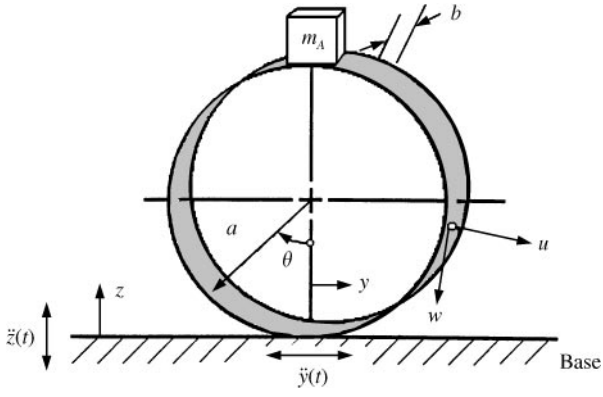

Figure 2. Circular ring structure.

Details of the derivation of Love's equation governing the vibration of a circular ring with a concentrated mass is outlined in Appendix A. Accordingly, the governing equations of motion for the tangential and the normal components of the ring displacement are given as

$$\frac{\partial^6}{\partial\theta^6} w_a(\theta, t) + 2\frac{\partial^4}{\partial\theta^4} w_a(\theta, t) + \frac{\partial^2}{\partial\theta^2} w_a(\theta, t) + \frac{a^4}{EI}\frac{\partial}{\partial\theta}\left[M_\rho \frac{\partial^3}{\partial\theta\,\partial t^2} w_a(\theta, t)\right]$$

$$-\frac{M_\rho a^4}{EI}\frac{\partial^2}{\partial t^2} w_a(\theta, t) = \frac{a^4}{EI}\left(-q_w - \frac{\partial q_u}{\partial\theta}\right), \tag{1}$$

$$\frac{\partial}{\partial\theta} w_a(\theta, t) = -u_a(\theta, t), \tag{2}$$

where w_a is the tangential deflection, u_a is the radial deflection, θ is the angle measured from the vertical, t is time, EI represents the bending stiffness, a is the ring radius, q_w is an external tangential force per unit length and q_u is an external normal force per unit length. The mass distribution of the ring (including the concentrated mass located at the top of the ring) per unit length is given as [31]

$$M_\rho = \rho A + \frac{m_A}{2\pi a}\,\delta(\theta - \pi), \tag{3}$$

where ρ is the mass density of the ring, A is the cross-sectional area, m_A is the mass of the avionics box represented by a concentrated mass located at $\theta = \pi$ and $\delta(\ )$ denotes the Dirac delta function.

3. FREE VIBRATION OF A RING

The natural frequencies of the ring are obtained by solving the homogenous form of equation (1) (in the absence of the concentrated mass at the top of the ring). Assuming a solution of the form [28]

$$w_a(\theta, t) = W(\theta)\,\mathrm{e}^{\mathrm{i}\omega t}, \tag{4}$$

the resulting equation may be restated as

$$\frac{\mathrm{d}^6 W}{\mathrm{d}\theta^6} + 2\,\frac{\mathrm{d}^4 W}{\mathrm{d}\theta^4} + \frac{\mathrm{d}^2 W}{\mathrm{d}\theta^2}\,(1 - \Omega^2) + \Omega^2 W = 0, \tag{5}$$

where

$$\Omega^2 = \frac{\omega^2}{\omega_0^2} \quad \text{and} \quad \omega_0^2 = \frac{EI}{\rho A a^4}. \tag{6}$$

The appropriate boundary conditions are

$$\begin{aligned} W(\theta) &= 0 \\ -U(\theta) = \frac{\mathrm{d}W(\theta)}{\mathrm{d}\theta} &= 0 \quad \text{at } \theta = 0 \quad \text{and at} \quad \theta = 2\pi. \\ \frac{\mathrm{d}^2 W(\theta)}{\mathrm{d}\theta^2} &= 0 \end{aligned} \tag{7}$$

The solution to equation (5) is given by

$$W(\theta) = \sum_{j=1}^{6} C_j\,\mathrm{e}^{\lambda_j \theta}, \tag{8}$$

where the C_j's are found using the boundary conditions given by equation (7) and the λ_j's are the roots of the dispersion equation given as

$$\lambda^6 + 2\lambda^4 + \lambda^2(1 - \Omega^2) + \Omega^2 = 0. \tag{9}$$

TABLE 1

Ring Properties

Modulus, E	199×10^2 N/m^2
The Poisson ratio, μ	0·3
Radius, a	0·07104 m
Thickness, h	$5{\cdot}1 \times 10^{-4}$ m
Width, b	0·03165 m
Top mass, m	0·450 kg
Density, ρ	7916 kg/m^3

TABLE 2

Analytical ring natural frequencies and damping values

Mode	1	2	3	4	5	6
f_j (Hz)	13·75	37·50	78·75	133·75	202·50	282·50
ω_j (rad/s)	86·39	235·61	494·80	840·37	1272·34	1775·00
Ω_j	0·56642	1·59520	3·38459	5·75492	8·68973	12·13275
ζ_j	0·036	0·040	0·025	0·018	0·025	0·019

When the boundary conditions are applied to the solution given by equation (8), a group of six simultaneous equations are obtained. In matrix form, these equations are expressed as

$$\begin{bmatrix} 1 & 1 & 1 & 1 & 1 & 1 \\ \lambda_1 & \lambda_2 & \lambda_3 & \lambda_4 & \lambda_5 & \lambda_6 \\ \lambda_1^2 & \lambda_2^2 & \lambda_3^2 & \lambda_4^2 & \lambda_5^2 & \lambda_6^2 \\ e^{2\lambda_1\pi} & e^{2\lambda_2\pi} & e^{2\lambda_3\pi} & e^{2\lambda_4\pi} & e^{2\lambda_5\pi} & e^{2\lambda_6\pi} \\ \lambda_1 e^{2\lambda_1\pi} & \lambda_2 e^{2\lambda_2\pi} & \lambda_3 e^{2\lambda_3\pi} & \lambda_4 e^{2\lambda_4\pi} & \lambda_5 e^{2\lambda_5\pi} & \lambda_6 e^{2\lambda_6\pi} \\ \lambda_1^2 e^{2\lambda_1\pi} & \lambda_2^2 e^{2\lambda_2\pi} & \lambda_3^2 e^{2\lambda_3\pi} & \lambda_4^2 e^{2\lambda_4\pi} & \lambda_5^2 e^{2\lambda_5\pi} & \lambda_6^2 e^{2\lambda_6\pi} \end{bmatrix} \begin{bmatrix} C_1 \\ C_2 \\ C_3 \\ C_4 \\ C_5 \\ C_6 \end{bmatrix} = 0. \tag{10}$$

A non-trivial solution for the C_j exist only if the determinant of the coefficient matrix in equation (10) is zero.

An iterative procedure is used to find the natural frequencies and the corresponding modal coefficients. An initial guess for the frequency (Ω) is made and then the λ_j's are computed from equation (9). Using these λ_j's, the determinant of the coefficient matrix (10) is evaluated. If the determinant does not become zero, then the initial frequency guess is adjusted and the process is repeated until the determinant approaches zero. The mode shape coefficients, C_i, are then evaluated for each natural frequency using equation (10) and choosing $C_6 = 1$. The modal coefficients are then normalized for each mode such that

$$\sqrt{\sum_{j=1}^{6} C_j^2} = 1. \tag{11}$$

Using the dimensions and physical properties for the circular ring given in Table 1, equations (9) and (10) are evaluated for Ω, ω_j and λ_j. The modal frequencies and corresponding Ω_j's are listed in Table 2. Due to the complex form of the λ_j's obtained,

TABLE 3

Ring mode shape coefficients and parameters

Mode	i	a_i	b_i	C_i	Mode	i	a_i	b_i	C_i
	1	0·00	1·30876	− 0·10096		1	0·00	1·68930	− 0·11704
	2	0·38027	0·53683	− 0·14731		2	0·82800	0·50863	− 0·07916
1	3	− 0·38027	0·53683	− 0·01967	2	3	− 0·82800	0·50863	0·00077
	4			0·03524		4			− 0·00245
	5			0·12062		5			0·11626
	6			0·42328		6			0·45340
	1	0·00	2·17382	− 0·09447		1	1·99490	0·00	0·79760E-6
	2	1·20824	0·31161	− 0·05741		2	1·07927	0·00	− 0·22151
3	3	− 1·2082	0·31161	0·00033	4	3	0·00	2·67291	− 0·00033
	4			0·00018		4			0·29688
	5			0·09413		5			− 0·07503
	6			0·76404		6			− 0·04531
	1	2·65515	0·00	− 0·65433E-8		1	3·24700	0·00	0·11063E-9
	2	1·02932	0·00	− 0·11509		2	1·01428	0·00	− 0·08019
5	3	0·00	3·17952	0·00027	6	3	0·00	3·68399	− 0·00022
	4			0·17655		4			0·13268
	5			− 0·06173		5			− 0·05225
	6			− 0·03904		6			− 0·03409

equation (8) may be stated as

$$W_k(\theta) = \begin{cases} \sum_{i=1}^{3} (C_{2i-1,k} e^{a_{i,k}\theta} \cos b_{i,k}\theta + C_{2i,k} e^{a_{i,k}\theta} \sin b_{i,k}\theta) & \text{for } k = 1,\ 2,\ 3, \\ \sum_{i=1}^{2} (C_{2i-1,k} e^{a_{i,k}\theta} + C_{2i,k} e^{-a_{i,k}\theta}) + C_{5,k} \cos b_{3,k}\theta + C_{6,k} \sin b_{3,k}\theta & \text{for } k = 4,\ 5,\ 6. \end{cases} \tag{12}$$

The mode shape coefficients and parameters for equation (12) that were found using the frequencies and λ_j's from equations (9) and (10) are listed in Table 3 and the corresponding mode shapes are shown in Figure 3. The mode shapes are categorized according to their motion at the top of the ring ($\theta = \pi$), either lateral or vertical. The odd-numbered modes exhibit predominantly side-to-side motion and are thereby called lateral modes. Whereas the even-numbered modes have mostly an up and down response and therefore are labelled vertical modes. Only the first six modes are shown and used in the calculations.

4. RING RESPONSE DUE TO BASE EXCITATION

In this section, the response of a circular ring, shown in Figure 2, subjected to base excitation is analyzed. The absolute motion of the ring is assumed to be given as

$$w_a(\theta, t) = w(\theta, t) - y(t) \cos\theta + z(t) \sin\theta \tag{13}$$

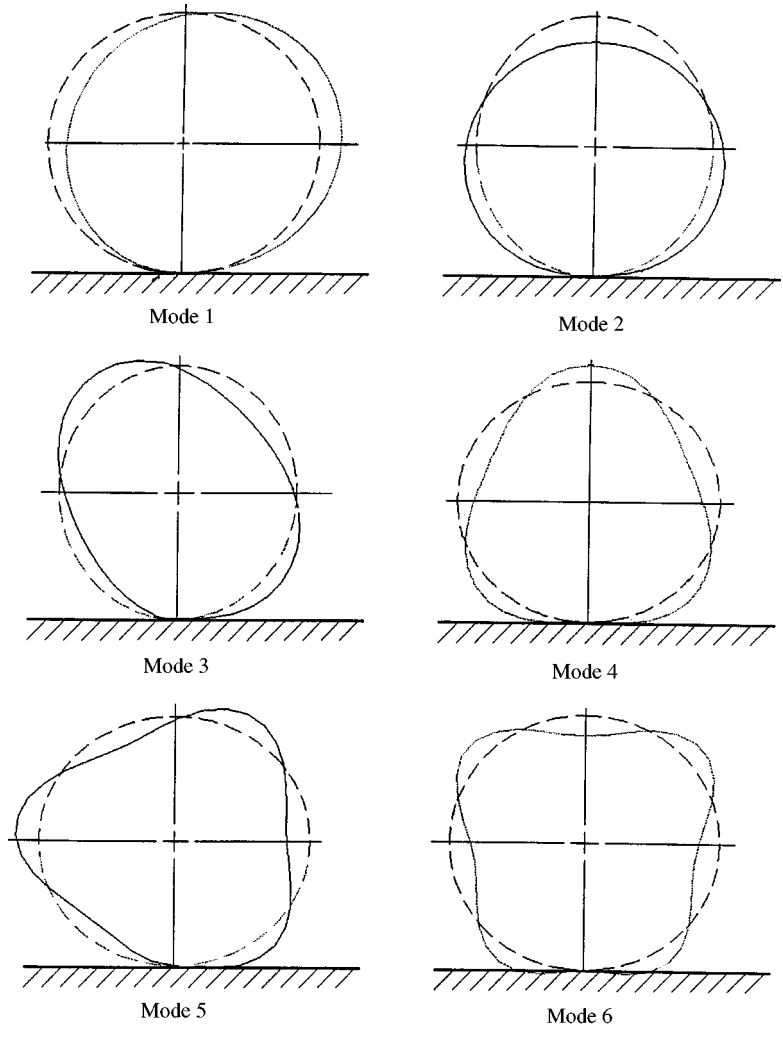

Figure 3. Circular ring mode shapes.

and

$$u_a(\theta, t) = u(\theta, t) - y(t) \sin \theta - z(t) \cos \theta, \tag{14}$$

where u and w are relative, normal and tangential, ring displacements and y and z are base displacements.

The motion of the ring relative to the base is assumed to be given by

$$w(\theta, t) = \sum_k \eta_k(t) W_k(\theta) \tag{15}$$

and

$$u(\theta, t) = \sum_k \eta_k(t) U_k(\theta). \tag{16}$$

Substituting equations (3), (13) and (15) into equation (1) yields

$$\frac{\partial^6}{\partial\theta^6}\sum_k \eta_k(t)\,W_k(\theta) + 2\,\frac{\partial^4}{\partial\theta^4}\sum_k \eta_k(t)\,W_k(\theta) + \frac{\partial^2}{\partial\theta^2}\sum_k \eta_k(t)\,W_k(\theta)$$
$$+ \frac{a^4}{EI}\,\frac{m_a}{2\pi a}\,\delta'(\theta-\pi)\left(\sum_k \ddot{\eta}_k(t)\,\frac{\mathrm{d}W_k}{\mathrm{d}\theta} + \ddot{y}(t)\sin\theta + \ddot{z}(t)\cos\theta\right)$$
$$+ \frac{a^4}{EI}\left(\rho A + \frac{m_a}{2\pi a}\,\delta(\theta-\pi)\right)\left(\sum_k \ddot{\eta}_k(t)\,\frac{\mathrm{d}^2W_k}{\mathrm{d}\theta^2} - \sum_k \ddot{\eta}_k(t)\,W_k + 2\ddot{y}(t)\cos\theta - 2\ddot{z}(t)\sin\theta\right)$$
$$= \frac{a^4}{EI}\left(-q_w - \frac{\partial q_u}{\partial\theta}\right). \tag{17}$$

Using the relation given by equation (5) in equation (17) and simplifying yields

$$\sum_k \left\{(\ddot{\eta}_k + w_k^2\eta_k)\left(W_k - \frac{\mathrm{d}^2W_k}{\mathrm{d}\theta^2}\right) + \frac{m_A}{2\pi\rho Aa}\,\ddot{\eta}_k\left[\left(W_k - \frac{\mathrm{d}^2W_k}{\mathrm{d}\theta^2}\right)\delta(\theta-\pi) - \frac{\mathrm{d}W_k}{\mathrm{d}\theta}\,\delta'(\theta-\pi)\right]\right\}$$
$$= \frac{1}{\rho A}\left(q_w + \frac{\partial q_u}{\partial\theta}\right) + \left(1 + \frac{m_A}{2\pi\rho Aa}\,\delta(\theta-\pi)\right)(2\ddot{y}(t)\cos\theta - 2\ddot{z}(t)\sin\theta)$$
$$+ \frac{m_A}{2\pi\rho Aa}\,\delta'(\theta-\pi)\,(\ddot{y}(t)\sin\theta + \ddot{z}(t)\cos\theta). \tag{18}$$

Multiplying equation (18) by a normal mode, W_p, integrate around the ring and apply the orthogonality condition given by

$$\int W_p\left(W_k - \frac{\mathrm{d}^2W_k}{\mathrm{d}\theta^2}\right)\mathrm{d}\theta = 0, \quad k \neq p, \tag{19}$$

we find

$$\ddot{\eta}_p + 2\zeta_p w_p\dot{\eta}_p + \omega_p^2\eta_p + K_p = F_p + B_{p_y}\ddot{y}(t) + B_{p_z}\ddot{z}(t), \tag{20}$$

where

$$\zeta_p = \frac{\gamma}{2\rho A\omega_p} \tag{21}$$

is the modal damping coefficient, γ is an equivalent viscous damping factor introduced into equation (20), η_p is the modal participation factor, ω_p is the pth natural frequency, $\ddot{z}(t)$ is the vertical base excitation and $\ddot{y}(t)$ is the lateral base excitation. The external pressure field is given by

$$q_w = 0 \quad \text{and} \quad q_u = \frac{m_A g}{2\pi a}\,\delta(\theta-\pi), \tag{22}$$

where $m_A g$ is the static weight at the top of the ring.

The coefficients in equation (20) are then defined as follows:

$$K_p = \frac{m_A}{2\pi\rho A a N_p} \sum_k \ddot{\eta}_k \left(W_k(\pi)\, W_p(\pi) + \frac{\mathrm{d}W_k(\pi)}{\mathrm{d}\theta} \frac{\mathrm{d}W_p(\pi)}{\mathrm{d}\theta} \right), \tag{23}$$

$$F_p = -\frac{m_A g}{2\pi\rho A a N_p} \frac{\mathrm{d}W_p(\pi)}{\mathrm{d}\theta}, \tag{24}$$

$$B_{p_y} = \frac{1}{N_p} \left(2 \int_\theta W_p(\theta) \cos\theta \, \mathrm{d}\theta - \frac{m_A}{2\pi\rho A a} W_p(\pi) \right), \tag{25}$$

$$B_{p_z} = \frac{1}{N_p} \left(-2 \int_\theta W_p(\theta) \sin\theta \, \mathrm{d}\theta + \frac{m_A}{2\pi\rho A a} \frac{\mathrm{d}W_p(\pi)}{\mathrm{d}\theta} \right), \tag{26}$$

where

$$N_p = \int_\theta \left(W_p^2(\theta) - \frac{\mathrm{d}^2 W_p(\theta)}{\mathrm{d}\theta^2} W_p(\theta) \right) \mathrm{d}\theta \tag{27}$$

is the norm of the pth modal amplitude.

The equations given in equation (20) are coupled since K_p depends on $\sum_k \ddot{\eta}_k(t)$. Here, a Gaussian reduction scheme is used to solve the equations simultaneously for the modal participation factors in the numerical simulation.

5. EXCITATIONS

Both sinusoidal and random base excitations are used to evaluate the performance of the passive vibration isolation system. Sinusoidal base accelerations applied are given by

$$\ddot{y}(t) = Y_a \sin(\omega_e t) \quad \text{and} \quad \ddot{z}(t) = Z_a \sin(\omega_e t), \tag{28}$$

where Y_a and Z_a are the amplitudes, ω_e is the excitation frequency and t is time. The base accelerations, $\ddot{y}(t)$ and $\ddot{z}(t)$, are used in the following analyses.

The random excitation being used is modelled after NASA Ames/Dryden Flight Research Facility (ADFRF) process specification No. 21-2 for environmental testing of electronic and electromechanical equipment [32], as shown in Figure 4. The random excitation model uses the frequency sampling method to design a non-recursive finite impulse response (FIR) filter. As illustrated in Figure 5, zero-mean Gaussian white noise, $\varepsilon(t)$, is input to the filter (with impulse response $h(t)$), and the output being the random excitation, $\ddot{y}(t)$ or $\ddot{z}(t)$. That is,

$$\ddot{y}(t) = \int_0^t h(t-\tau)\, \varepsilon_y(\tau)\, \mathrm{d}\tau \quad \text{and} \quad \ddot{z}(t) = \int_0^t h(t-\tau)\, \varepsilon_z(\tau)\, \mathrm{d}\tau. \tag{29}$$

The mean and autocorrelation of the stationary, Gaussian white-noise processes, $\varepsilon_y(t)$ and $\varepsilon_z(t)$, used as the input are given as

$$\langle \varepsilon_y(t) \rangle = 0, \quad \langle \varepsilon_y(t_1) \varepsilon_y(t_2) \rangle = 2\pi S_{o_y} \delta(t_1 - t_2), \quad \langle \varepsilon_y(t_1)\, \varepsilon_z(t_2) \rangle = 0,$$

$$\langle \varepsilon_z(t) \rangle = 0, \quad \langle \varepsilon_z(t_1)\, \varepsilon_z(t_2) \rangle = 2\pi S_{o_z} \delta(t_1 - t_2), \tag{30}$$

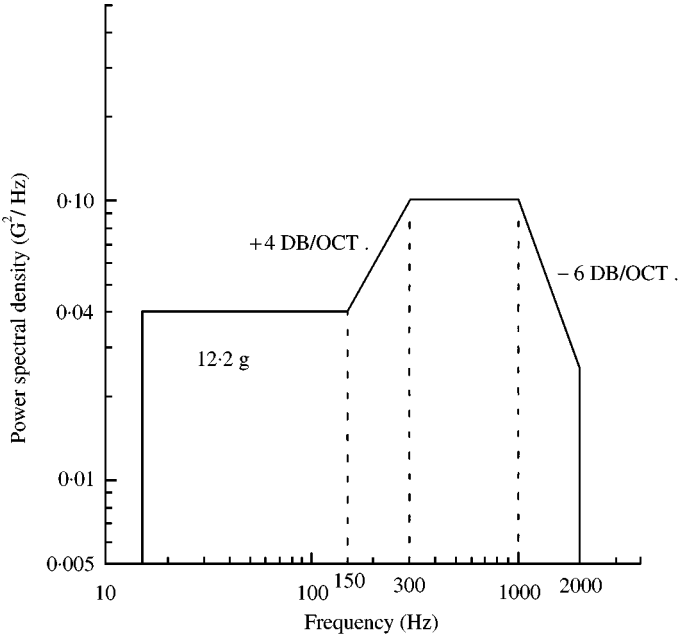

Figure 4. NASA ADFRF process specification No. 21-2.

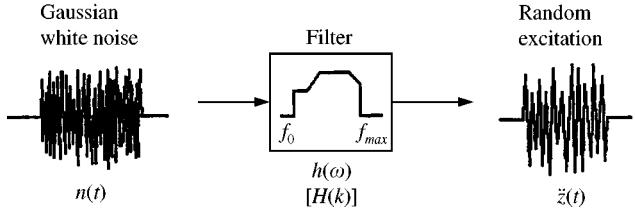

Figure 5. Random excitation model.

where the angular brackets, '$\langle \cdot \rangle$', represent ensemble averaging and S_{o_y} and S_{o_z} are the constant power spectral intensities. The spectral intensity of the white-noise excitations for the y and z directions are assumed to be given as

$$S_{o_y} = 0{\cdot}0043 \text{ g}^2 \text{ s}, \quad S_{o_z} = 0{\cdot}0218 \text{ g}^2 \text{ s}. \tag{31}$$

The value for $S_{o_z}$was estimated so that the spectral density of the vertical random excitation would fit that of the NASA ADFRF process specification. The lateral value was taken to be one-fifth the vertical value since the lateral excitation intensity is usually much lower than that of the vertical excitation in aircraft. The impulse response, $h(t)$, is obtained by inverse Fourier transform given as

$$h(t) = \Im^{-1}[H(k)], \tag{32}$$

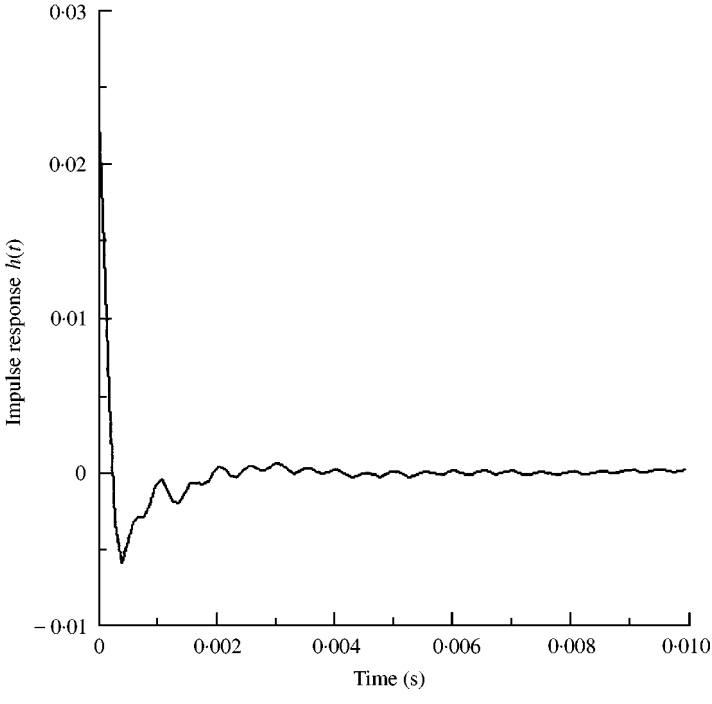

Figure 6. Impulse response function.

where $H(k)$ is the system function. The system function is a function of the acceleration power spectral density function represented in Figure 4 and given by

$$|H(k)| = \sqrt{\frac{N}{2\Delta t}\ \tilde{G}(k)}, \tag{33}$$

where N is the number of samples, Δt is the spacing between time samples and $\tilde{G}(k)$ is the power spectral density function.

To design a FIR filter with the frequency response shown in Figure 4, the frequency response is sampled N times at intervals of $k\ F_s/N$, $k = 0, 1, \ldots, N-1$, where F_s is the sampling frequency. Since these values are related to the Fourier transform of the filter impulse response, the filter coefficients $h(n)$ [$\equiv h(n\Delta t)$] are found using an inverse Fourier transform of the frequency samples from equation (33). For linear phase filters with a positive symmetrical impulse response, it is possible to rewrite the inverse Fourier transform such that the FIR filter coefficients are given by [33]

$$h(n) = \frac{1}{N}\left[\sum_{k=1}^{N/2-1} 2|H(k)|\cos|[2\pi k(n-\alpha)/N]| + H(0)\right], \tag{34}$$

where $H(k)$ are the frequency samples, $n = 0, \ldots, N-1$ and $\alpha = (N-1)/2$. Here $\Delta t = 0{\cdot}1$ s and $N = 1024$ samples are used. The impulse response of the above FIR filter is shown in Figure 6.

The fast Fourier transform (FFT) is used to transform the filter coefficients and white noise to the frequency domain. They are multiplied together and the result is inverse transformed using the inverse FFT back to the time domain. This produces time samples

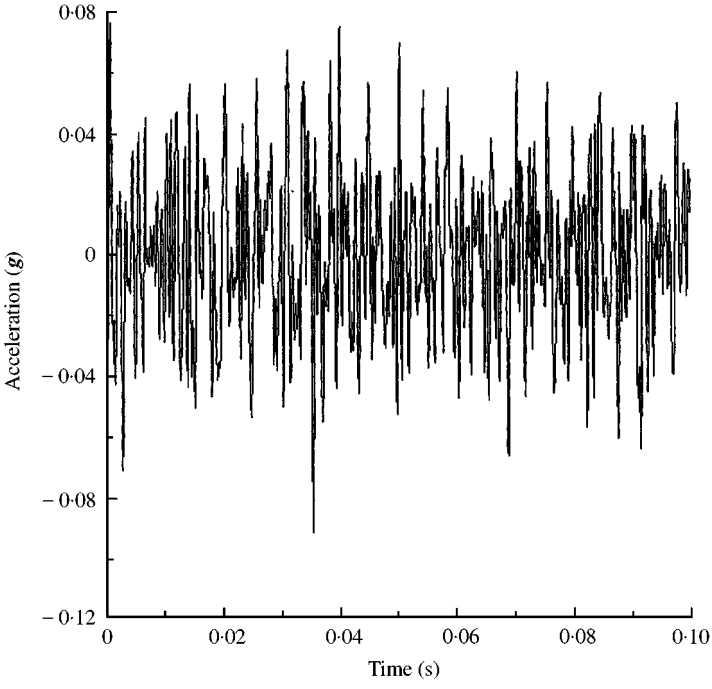

Figure 7. Sample excitation time history.

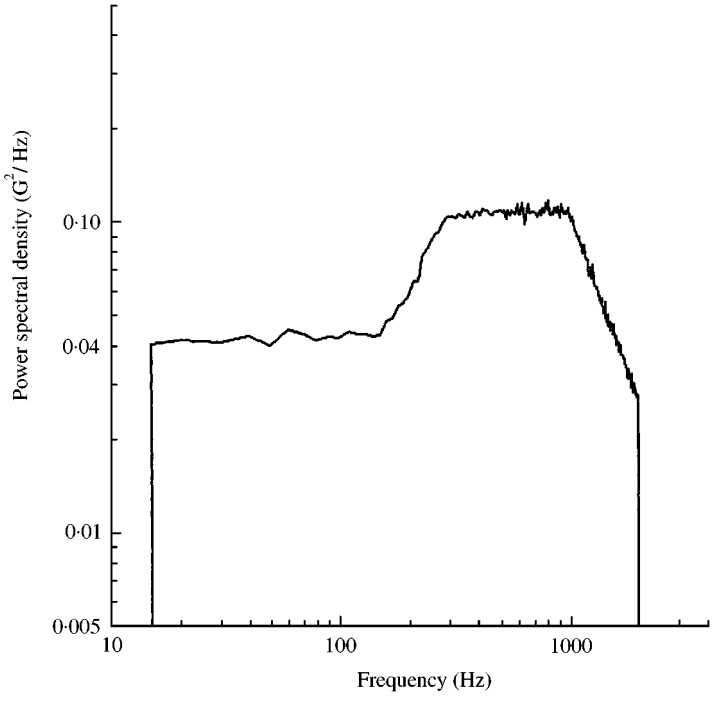

Figure 8. Power spectral density for an ensemble of 1000 time samples.

representative of the power spectral density shown in Figure 4. A sample simulated excitation time history is plotted in Figure 7. To verify that the procedure truly generates the appropriate frequency response, an ensemble of 1000 sample time histories were generated, transformed to the frequency domain and the averaged spectrum, $(1/T)|\bar{\bar{z}}(\omega)|^2$, was evaluated. The resulting response power spectral density is shown in Figure 8. Comparing Figures 4 and 8, it is observed that the filter produces time samples representative of the desired excitation spectrum.

6. EXPERIMENT

The purpose of the experiment was to measure the natural frequencies and damping of a circular steel ring for comparison with the analytical results. The experimental set-up is shown schematically in Figure 9. The dimensions and physical properties of the circular ring that was used in the experiment are the same as those listed in Table 1 and used in the analysis. Two 5-mm holes were drilled in the ring, one at the top and one at the bottom. The ring was bolted directly to the shaker armature through the bottom hole for both the vertical and lateral vibration testing. For rings with the concentrated mass test conditions, a steel weight was bolted through the hole at the top of the ring. Accelerometer mounting wax was used to hold the accelerometer onto the ring. The accelerometer was mounted on top of the ring for measuring vertical modes of vibration and on the side of the ring for measuring lateral modes. Five test conditions were evaluated for various concentrated masses. The concentrated masses used were 0, 130, 250, 430 and 780 g. (The accelerometer mass was negligibly small, and hence there was no need for a correction.)

The test system that was used to perform the experiment was entirely PC based. An A–D/D–A interface on the PC allowed the computer to output the shaker drive signal and monitor the system response channels. Software was used for FFT processing and vibration analysis. Broadband random excitation from 0 to 2000 Hz was generated by the computer and used to shake the ring vertically. A force transducer was installed between the ring and shaker rod in order to measure the input excitation. An accelerometer was mounted on top of the ring to measure the vertical acceleration. The accelerometer and force data were recorded using the PC-based data acquisition system. Twenty-five samples were acquired and averaged to produce the acceleration frequency response function (AFRF) for the vertical excitation for each test condition. Acceleration frequency response function (AFRF) is defined as the amplitude of the acceleration power spectral density normalized by the excitation intensity.

The lateral modes were measured using impact excitation. A small hammer was used to impact the side of the ring. An accelerometer mounted on the opposite side of the ring

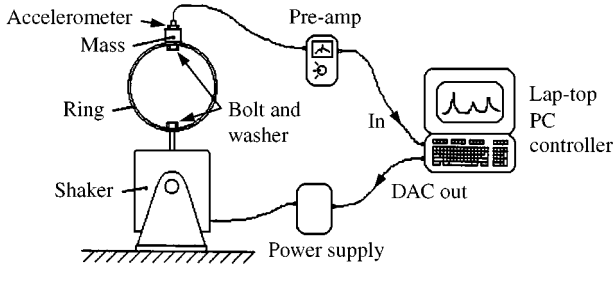

Figure 9. Experiment set-up for circular ring vibration.

TABLE 4

Experimental ring natural frequencies and damping values

Mass (g)	Mode	1	2	3	4	5	6
0	ω_j	86·394	229·336	507·367	854·513	1253·49	1790·71
	ζ_j	0·036	0·040	0·025	0·018	0·025	0·019
130	ω_j	31·416	83·252				
	ζ_j	0·056	0·057				
250	ω_j	21·991	69·115				
	ζ_j	0·112	0·036				
430	ω_j	18·850	53·407				
	ζ_j	0·120	0·053				
780	ω_j	12·566	39·270				
	ζ_j	0·091	0·060				

measured the ring response due to the impact. The response was recorded on the PC. Ten impact samples were measured and averaged and used to compute the power spectra for the lateral vibration data for each test condition. The experimental FRF's and power spectra were curve fit at each resonance frequency and the half-power bandwidth method was used to evaluate the modal damping. For a ring with no concentrated mass, the natural frequency and modal damping for the first six modes of the ring are listed in Table 4. For each of the test conditions with the concentrated mass attached to the ring, the two lowest modes are listed. Comparing Tables 2 and 4, it is observed that the computed natural frequencies are in close agreement with the experimental ones.

7. RESULTS

Computer simulation of the ring response is performed by solving equations (13)–(16) and equation (20) subjected to random base excitations. A typical circular ring with the dimensions and physical properties given in Table 1 is analyzed. The ring fundamental frequency is 13·75 Hz with a damping ratio of 0·036. Two ring configurations, one without any concentrated mass and one with a 0·45 kg mass added on top of the ring, are examined. The ring deflection is given by

$$u = u_s + u_e, \tag{35}$$

where u_s is the static deflection under the weight and u_e is the deflection relative to the static equilibrium. In this section, the vibration of the ring about the static equilibrium is studied. The static deflection, u_s, results from the gravitational force term given by equation (24). To achieve this in the numerical simulation, equation (20) is evaluated in the absence of base excitation, i.e.,

$$\eta_p = \frac{F_p}{\omega_p^2}. \tag{36}$$

This equation is evaluated and the modal participation factors are recorded. These values then establish the static equilibrium position of the ring due to the concentrated mass and

can be calculated using equations (2), (12), (16) and

$$u_s(\theta, t) = \sum_p \eta_p(t)\, U_p(\theta). \tag{37}$$

Subsequent analyses are then conducted using this static equilibrium position as a starting point. The stored values are used as initial conditions for solving equation (20) under base excitation.

Using both sinusoidal and random excitations, the acceleration at the top of the ring and the response of a (s.d.o.f.) system attached to the top of the ring are evaluated. The peak responses of the ring are computed for a range of ring frequencies. To assess the effectiveness of the base isolation at the point on the ring where the equipment is attached, acceleration response spectra are evaluated. The lateral and vertical acceleration response spectra are, respectively, defined as

$$S_a(\omega_a, \zeta_a) = \max_t \{|\ddot{w}_a(\pi, t)|\} \tag{38}$$

and

$$S_a(\omega_a, \zeta_a) = \max_t \{|\ddot{u}_a(\pi, t)|\}. \tag{39}$$

For random excitation, the mean, the standard deviation, the absolute maximum and the absolute minimum acceleration are defined, respectively, as

$$\bar{a}(\omega_a, \zeta_a) = \langle S_a(\omega_a, \zeta_a)\rangle, \tag{40}$$

$$\sigma_a(\omega_a, \zeta_a) = \langle (S_a(\omega_a, \zeta_a) - \bar{a})^2 \rangle^{1/2}, \tag{41}$$

$$a_{max}(\omega_a, \zeta_a) = \max\{S_a(\omega_a, \zeta_a)\}, \tag{42}$$

$$a_{min}(\omega_a, \zeta_a) = \min\{S_a(\omega_a, \zeta_a)\}. \tag{43}$$

It should be noted that the absolute maximum and minimum accelerations, which represent upper and lower bounds on the simulation results, are sample dependent.

8. COMPARISON OF NUMERICAL AND EXPERIMENTAL RESULTS

8.1. RING WITHOUT CONCENTRATED MASS

In order to verify the validity of the numerical model, the analytical ring response is computed in the same manner as was done in the experiment. Random excitation given by equation (29) is used to excite the ring in both lateral and vertical directions. The response at the top of the ring is computed and used with the input base excitation to generate vertical and lateral acceleration frequency response functions as shown in Figures 10 and 11 respectively. The experimental acceleration frequency response functions are also plotted in these figures for comparison. As noted before, the acceleration frequency response functions are defined as the amplitude of the acceleration power spectral density normalized by the intensity of the excitation. The exception is the experimental result for the lateral excitation shown in Figure 11, which was obtained by an impact hammer and was not normalized. (NN denotes "not normalized" in this figure.) The peaks in each frequency response function correspond to the natural frequencies of the ring as listed in Table 2. The damping

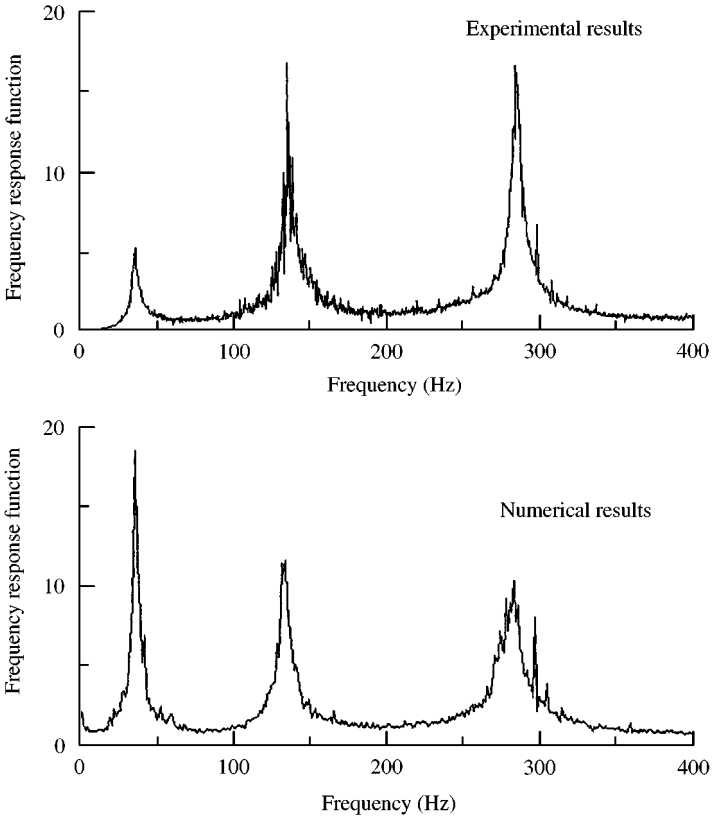

Figure 10. Comparison of analytical and experimental acceleration frequency response functions for the circular steel ring for vertical excitation.

values that were calculated from the experimental data as listed in Table 4 were used in the analytical model.

Figures 10 and 11 show reasonable general agreement between the experimental and the numerical acceleration frequency response functions. However, the peak value amplitudes at the resonant frequencies are not in agreement. Part of the differences in peak amplitudes may be due to the frequency response of the accelerometer used. The accelerometer is rated for an operating range of 10–10 000 Hz. The accelerometer frequency response is levelled down to about 100 Hz. However, the response starts to roll off below 100 Hz and the accelerometer is unusable below about 10 Hz. Therefore, the amplitude of the experimental resonant frequencies below 100 Hz are attenuated for both the vertical and lateral results. Additional experimental inaccuracy and the slight error in the estimate of damping coefficient could also be the cause of the observed discrepancy in the higher modes. It should be noted here that the peak response amplitudes of the lateral vibration results should not be compared directly. As was noted before, the experimental results were acquired with the impact excitation and the corresponding acceleration frequency function was not normalized. The numerical results, however, were generated with a random white-noise excitation and the corresponding response power spectral density was normalized by the intensity of the excitation for evaluating the acceleration frequency response function. This was due to the experimental shaker limitation that was not able to generate white-noise excitation in the lateral direction.

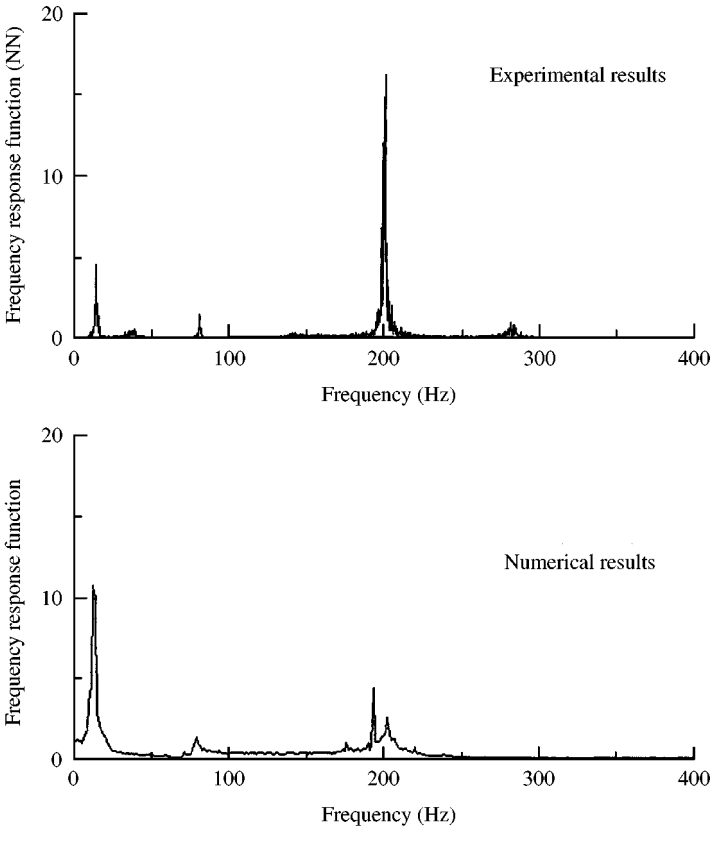

Figure 11. Comparison of analytical acceleration frequency response function and experimental power spectral density for the circular steel ring for lateral excitation.

8.2. RING WITH RIGID AVIONICS

Next, the circular ring with a 0·45 kg rigid avionics mass attached to its top is analyzed. The ring response is computed in the same manner as outlined above for Figures 10 and 11. Random excitation given by equation (29) is used to excite the ring in both the lateral and vertical directions. Vertical and lateral acceleration frequency response functions are plotted in Figures 12 and 13. The corresponding experimental frequency response functions are also shown in these figures for comparison. The ring geometry is the same as that used earlier with the exception of the additional mass. Comparing Figures 10 and 11 with Figures 12 and 13, it is noticed that the ring natural frequencies are lower with the additional mass on top as expected. Both experimental and numerical results indicate a decrease in the natural frequencies with fairly close agreement between the two. The observed variations in the resonant frequency peak amplitudes are due to accelerometer frequency response characteristics and for the lateral case, are also due to the different methods of excitation used. Numerical results for the lateral case are produced with random excitation whereas impact excitation is used in the experiment. Figures 12 and 13 show qualitative agreement in overall trends between the experimental and numerical data.

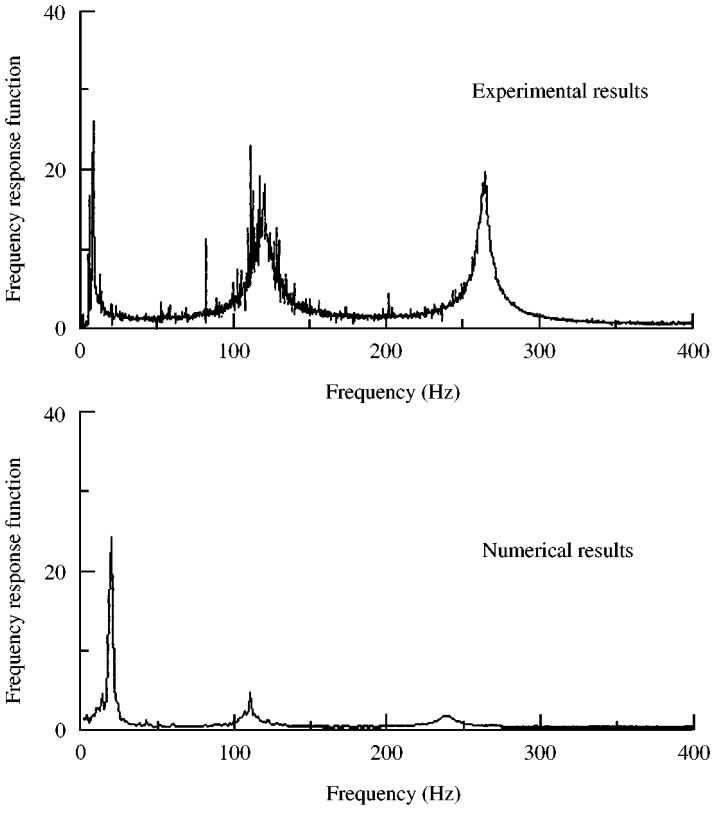

Figure 12. Comparison of analytical and experimental acceleration frequency response functions for the circular steel ring with a 0·45 kg concentrated mass under vertical random base excitation.

8.3. AVIONICS BOX UNDER SINUSOIDAL EXCITATION

In this section, responses of a s.d.o.f. avionics box subject to horizontal–vertical sinusoidal base excitation with and without a ring isolation system are studied. Figure 14 illustrates the system configurations considered. Sinusoidal base excitation, as given by equation (28), is used. The amplitude, A, of the input excitation is 0·01 g in the vertical direction and 0·002 g in the lateral direction. The excitation frequency, f_e, is 400 Hz. The peak responses of the system are computed for a range of avionics equipment system frequencies from 50 to 500 Hz. Table 1 lists the physical properties of the ring used in the analysis with the natural frequencies that appear in Table 2. The interaction of the avionics system and the ring is neglected in the following analyses since it is assumed that the avionics system is rigidly attached to the ring.

The vertical and lateral acceleration response spectra of the avionics system are plotted in Figures 15 and 16. The cases of unprotected avionics and avionics with the ring are shown. For the avionics with the ring, two different responses are shown. No interaction implies that there was no coupling between the avionics and ring degrees of freedom. The response at the top of the ring was computed and used as excitation to the s.d.o.f. avionics box. The rigid mass response implies that the avionics box is treated as a rigid mass of 0·45 kg. Both figures show a peak at the excitation frequency of 400 Hz due to the resonance of the s.d.o.f. system with the excitation frequency. The ring natural frequencies given in Table 2 are not

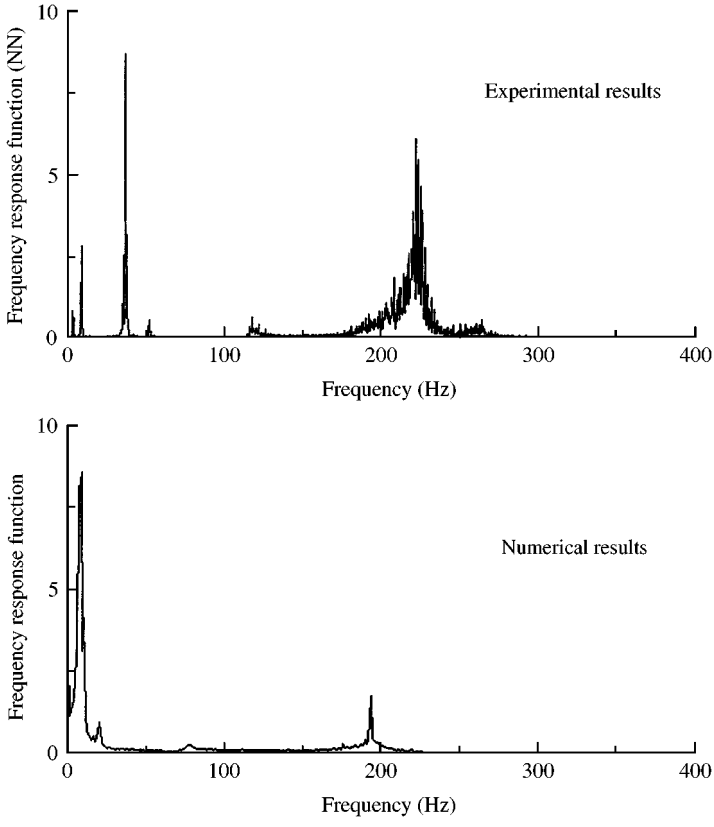

Figure 13. Comparison of analytical acceleration frequency response function and experimental power spectral density for the circular steel ring with a 0·45 kg concentrated mass under lateral random base excitation.

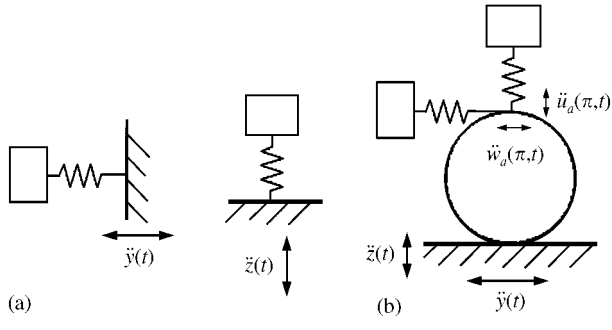

Figure 14. Single-degree-of-freedom system configurations: (a) s.d.o.f. system exposed to random excitation without ring, (b) s.d.o.f. system exposed to transmitted vibration at top of ring.

excited by the sinusoidal excitation as shown by the plots. For the vertical direction, there is a 50 per cent decrease in the transmitted acceleration to the avionics system on top of the ring with no interaction mass and an order of magnitude decrease for the rigid mass case as compared to the avionics system exposed directly to the sinusoidal excitation, unprotected avionics. Similar decreases are seen for the transmitted acceleration in the lateral direction.

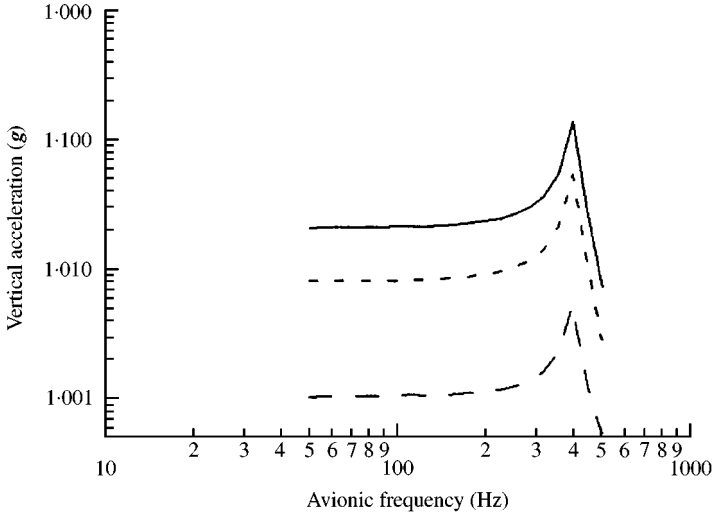

Figure 15. Comparison of vertical response spectra of an avionics system with and without the circular ring under sinusoidal base excitation: ——, unprotected avionics; – – –, avionics with ring (no interaction); — —, avionics with ring (rigid mass).

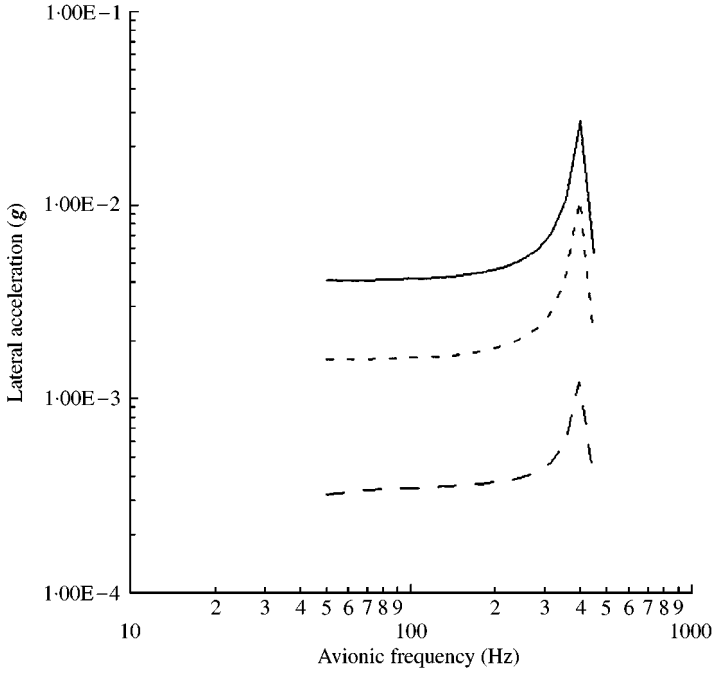

Figure 16. Comparison of lateral response spectra of an avionics system with and without the circular ring under sinusoidal base excitation: ——, unprotected avionics; – – –, avionics with ring (no interaction); — —, avionics with ring (rigid mass).

There is an order of magnitude decrease for the avionics system on the ring with no interaction mass and a one and a half order of magnitude decrease when the avionics on top of the ring is treated as a rigid mass. Clearly, the ring provides significant passive isolation for the avionics box.

8.4. RING RESPONSE TO RANDOM EXCITATION

For the case of a single ring (in the absence of a concentrated attached mass), the vertical ring response spectra for the top of the ring are plotted versus ring frequency in Figure 17 and the lateral response spectra are plotted in Figure 18. The peak responses for an ensemble of 100 samples are computed using the random excitation given by equation (29) and the results are compiled and the statistical response spectra are evaluated from equations (38) to (43). The input power spectra density level is 0·04 g^2/Hz up to 150 Hz and then increases at 4 DB/Oct to 0·10 g^2/Hz at 300 Hz as shown in Figures 4 and 8. Six modes are included in the numerical ring model. The mean vertical acceleration spectrum starts at about 0·002 **g** for a ring frequency of 15 Hz and increases over the frequency range plotted leveling off to about 0·025 **g** at a frequency of about 150 Hz. The mean lateral vibration starts off at about 0·0003 **g** at the lower frequencies (about 5 Hz) and steadily increases to about 0·003 **g** at a frequency of 60 Hz. This increase in acceleration is a result of the higher frequency modes responding to the increasing excitation levels The maximum and minimum acceleration levels are an extreme upper and lower bound, respectively, for the computed vibration spectrum.

To evaluate the effects of damping on ring performance, the vertical ring acceleration response spectra as a function of structural damping are calculated and plotted in Figure 19. The other ring parameters are as given in Table 1. The results are as expected, indicating a decrease in transmitted vibration with an increase in structural damping. It is observed from the graph that a damping value of about 6 per cent provides satisfactory isolation. For a passive ring system having 6 per cent damping as compared to that with a 2 per cent

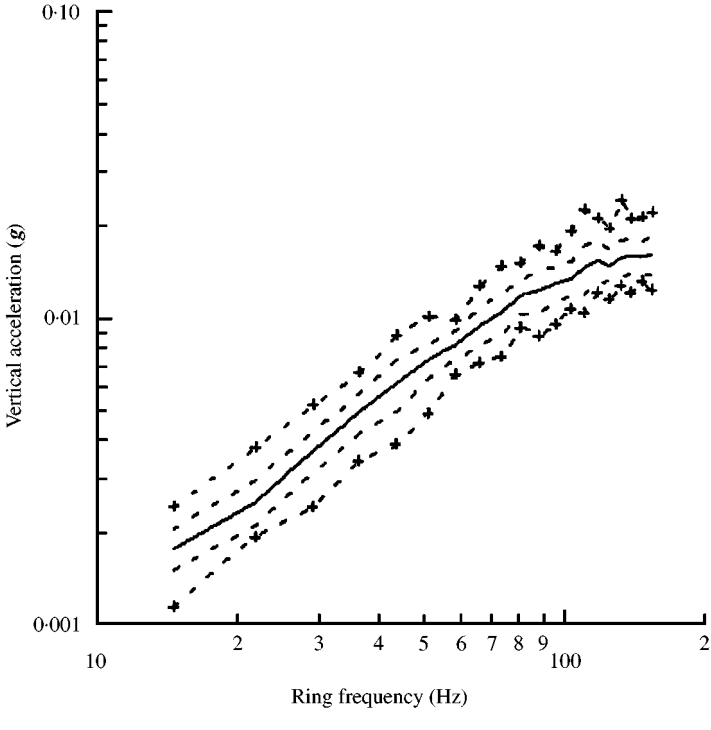

Figure 17. Statistical vertical response spectra of the circular ring without concentrated mass under random base excitation: + -- + , a_{max}; ----, $a + \sigma_a$; ——, $\bar{a}$; ----, $a - \sigma_a$; + -- + , a_{min}.

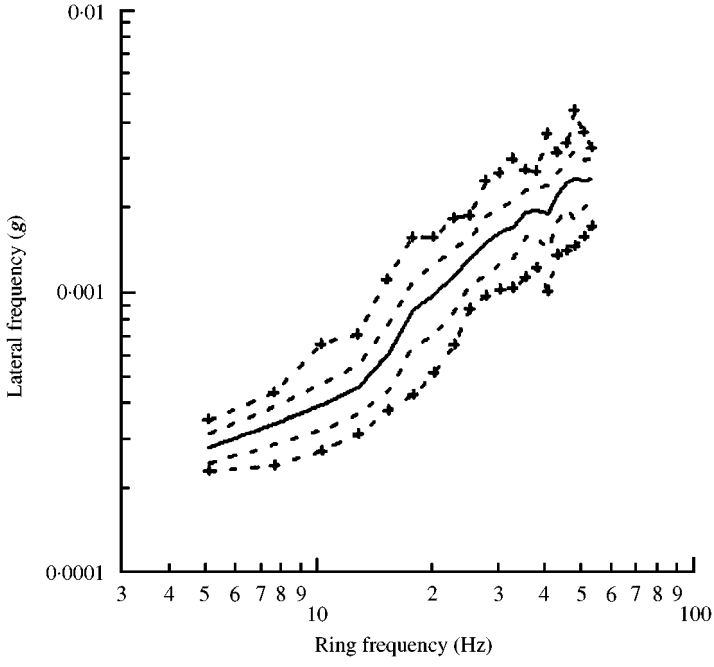

Figure 18. Statistical lateral response spectra of the circular ring without concentrated mass under random base excitation: + - - + , a_{max}; - - - -, $a + \sigma_a$; ——, $\bar{a}$; - - - -, $a - \sigma_a$; + - - + , a_{min}.

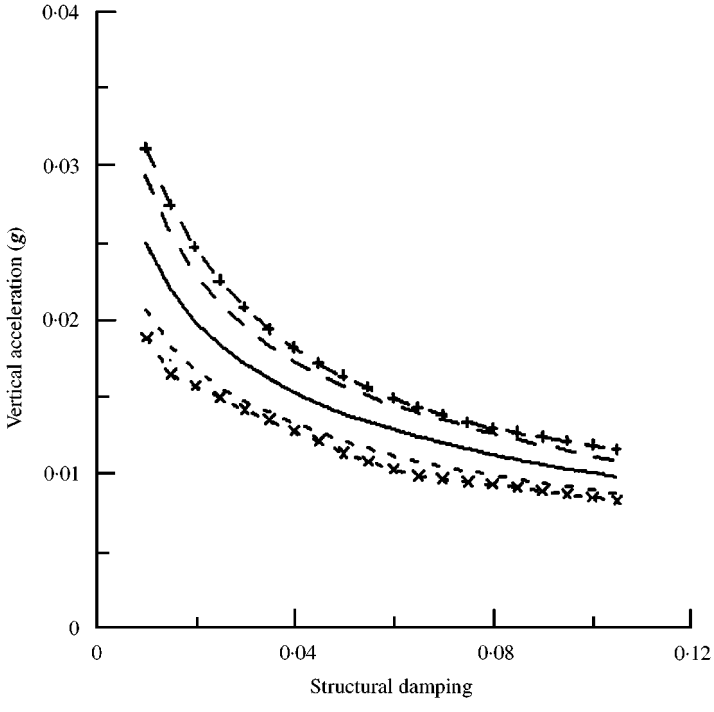

Figure 19. Statistical vertical response spectra of the circular ring as a function of damping under random base excitation: + - - + , a_{max}; – – –, $a + \sigma_a$; ——, $\bar{a}$; - - - -, $a - \sigma_a$; × - - ×, a_{min}.

damping, there is a 36 per cent decrease in transmitted excitation. Whereas another 4 per cent increase in damping above 6 per cent only provides an additional 14 per cent decrease in the transmitted vibration. Increasing the damping in the ring system above 10 per cent provides little if any improvement in the vibration environment at the top of the ring.

8.5. AVIONICS UNDER RANDOM EXCITATION

For the random base excitation, comparison is made between the acceleration responses of the avionics system mounted on top of the ring (treated as a rigid 0·45 kg concentrated mass) and the unprotected avionics system. The system response is computed for a range of avionics system frequencies from 50 to 500 Hz. The sensitivity to variations in the ring damping ratio on the response spectra is also examined. The resulting response spectra are plotted versus the avionics system frequency. As was noted before, the avionics system is treated as a rigid concentrated mass attached to the ring and the interaction between the avionics system and the ring is neglected.

The vertical and lateral avionics system acceleration response spectra with and without the ring are plotted in Figures 20 and 21. Comparing the response of the isolated avionics to that of the unprotected avionics, the transmitted vibration to the avionics system is cut in half using the ring as a passive isolator. When the avionics system is rigidly mounted on top of the ring, the acceleration levels are magnified at the ring natural frequencies as compared to the rest of the acceleration response. However, these levels are still considerably lower than the acceleration levels for the unprotected system. Even the maximum calculated acceleration levels of the isolated system are less than half the unprotected avionics

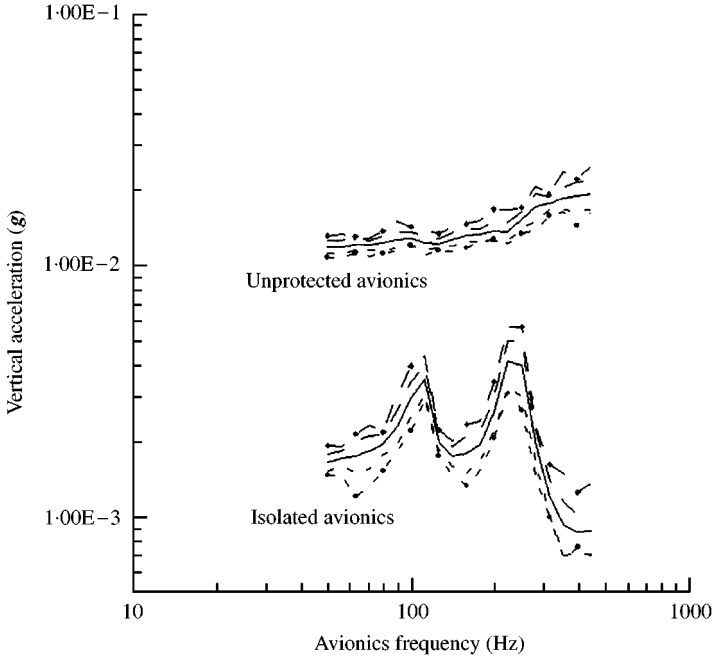

Figure 20. Comparison of vertical response spectra of avionics system with and without the circular ring under random base excitation—rigid mass avionics model: + -- + , a_{max}; – – –, $a + \sigma_a$; ——, $\bar{a}$; - - - -, $a - \sigma_a$; + -- + , a_{min}.

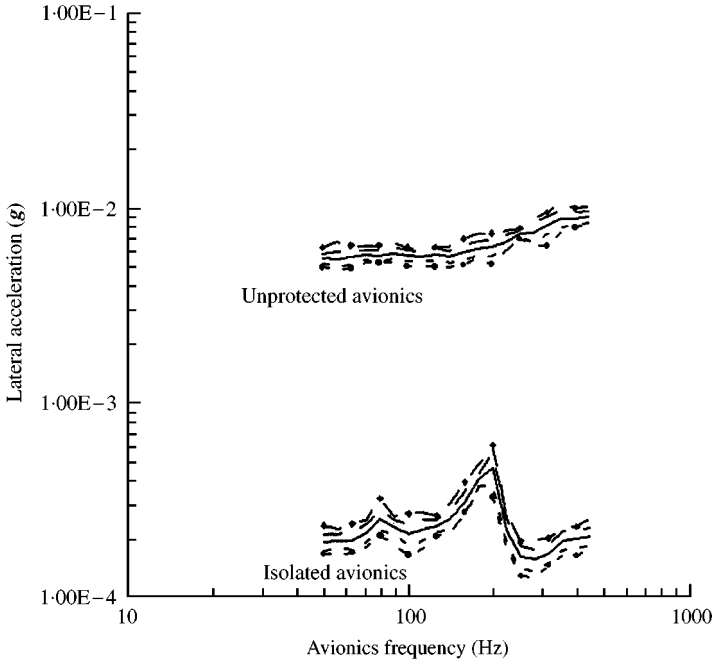

Figure 21. Comparison of lateral response spectra of avionics system with and without the circular ring under random base excitation—rigid mass avionics model: + - - + , a_{max}; - - - -, $a + \sigma_a$; ——, $\bar{a}$; - - - -, $a - \sigma_a$; + - - + , a_{min}.

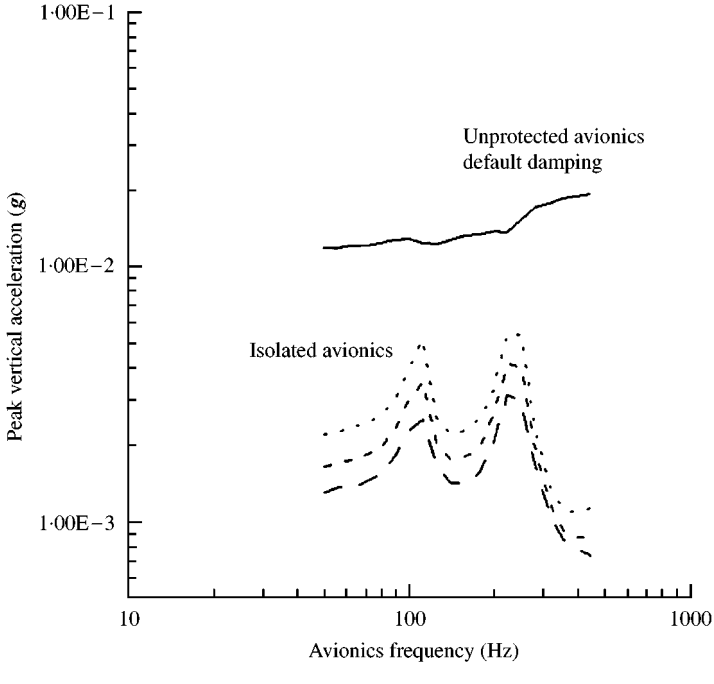

Figure 22. Vertical response spectra of an isolated avionics system with circular ring damping ratio variations as compared to unprotected avionics under random base excitation: Isolated avionics - - - -, −50%; – – –, default damping; ——, +100%.

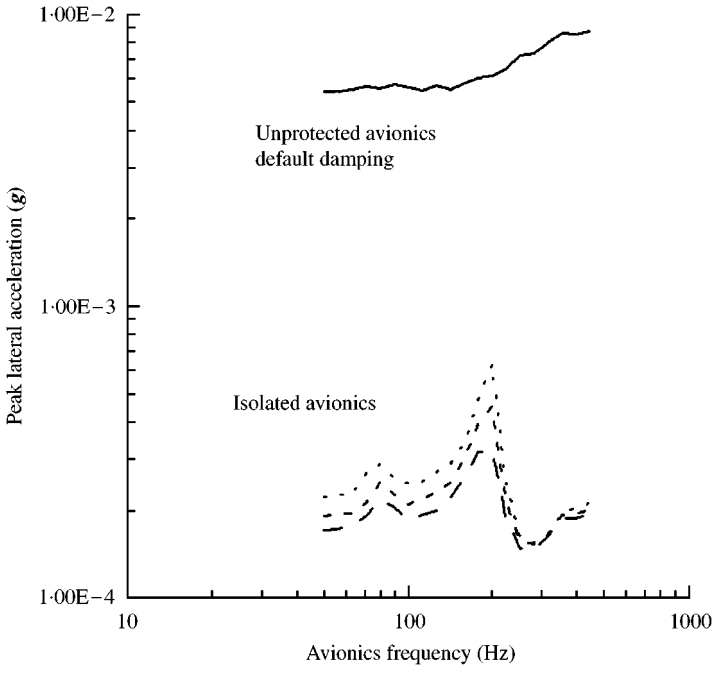

Figure 23. Lateral response spectra of an isolated avionics system with circular ring damping ratio variations as compared to unprotected avionics under random base excitation: Isolated avionics ----, −50%; – – –, default damping; ——, +100%.

minimum response. In the lateral direction, the ring isolates the avionics system by at least an order of magnitude over the entire frequency range. The isolated avionics response again is greater at the ring resonant frequencies as compared to the rest of the spectrum. The ring performs better in the lateral direction by not transmitting the lateral excitation into the avionics system as readily as the vertical excitation.

The peak acceleration response of the avionics system rigidly mounted to the ring is calculated for several damping ratios and plotted as a function of avionics frequency in Figures 22 and 23. These curves are compared to the response of the unprotected avionics system. The default damping values referred to in the figures are those listed in Table 2 with the 100% value being twice what is listed and −50% being half the listed value. As shown in both figures, the peak acceleration decreases with increasing structural damping. Again, the results are as expected. Increasing the ring damping increases the isolation effectiveness of the passive ring element and the peak acceleration levels for all damping values are less than the levels for the unprotected system.

9. CONCLUSIONS

An analytical model of a stainless-steel circular ring for the purpose of base isolation of avionics equipment is formulated. This model is used to evaluate the circular ring response characteristics subject to base excitation. Filtered zero-mean Gaussian white noise was tuned to match the NASA process specification No. 21-2 and is used for the random excitation. Peak acceleration response spectra are evaluated as a function of avionics frequency and ring structural damping. The ring is evaluated as an passive isolator for

a rigidly mounted avionics system. This system is compared to the response of the unprotected system. An experiment was performed to measure the modal response of the thin circular steel ring mounted on top of an electrodynamic shaker. The analytical ring responses closely match the experimental results. The peak avionics system acceleration spectra indicate that the ring is an effective isolator in both the vertical and lateral directions., the ring isolates the avionics system at all frequencies.

The sensitivity of the ring response and avionics system response to variations in ring parameters and additional mass on top of the ring is examined. With no added mass at the top of the ring, the peak ring acceleration increases with increasing excitation. Changes in structural damping produce expected results in peak ring acceleration; decreasing transmitted acceleration with increasing damping factor. Overall, the ring and avionics system responses were insensitive to small variations in ring properties [34].

It should be emphasized that the presented analysis was based on the in-plane motion of the ring. When several rings with different orientations as shown in Figure 1 are used, out-of-plane motion of rings will affect their vibration isolation performance. Consideration of the out-of-plane motion of the ring, however, is left for a future study.

ACKNOWLEDGMENTS

This work was supported by the NASA Dryden Flight Research Facility, Edwards, CA under the Grant No. NGT-51314.

REFERENCES

1. M. L. MUNJAL 1975 *Journal of Sound and Vibration* **39**, 247–263. A rational synthesis of vibration isolators.
2. J. C. SNOWDEN 1979 *Journal of the Acoustical Society of America* **66**, 1245–1279. Vibration isolation use and characterization.
3. R. PLUNKETT *Damping Applications for Vibration Control*, *Friction Damping*. ASME Booklet, Vol. AMD-38, 1980.
4. H. SUMALI and H. H. CUDNEY 1994 *35th Structures, Structural Dynamics, and Materials Conference*, *AIAA*-94-1466-*CP*. An active engine mount with a piezoelectric stacked actuator.
5. W. E. TRIPLETT, H. F. KAPPUS and R. J. LANDY 1973 *Air Force Flight Dynamics Laboratory*, *AFFDL-TR*-72-116. Active flutter suppression systems for military aircraft: a feasibility study.
6. G. S. AGNES, S. R. WHITEHOUSE and J. R. MACKAMAN 1993 *Proceedings of the Smart Structures and Materials Conference*, Vol. 1917(1), 368–379. Vibration attenuation of aircraft structures utilizing active materials.
7. R. E. GOGAN 1992 *INFLEX Final Report*. Harris Corporation, Melbourne, FL.
8. C. R. KNOSPE, R. D. HAMPTON and P. E. ALLAIRE 1991 *Acta Astronautica* **25**, 687–697. Control issues of microgravity vibration isolation.
9. G. LEE-GLAUSER and G. AHMADI 1991 *Clarkson Report No*. MIE-232. Dynamic response spectra for an aerospace payload and its attachment.
10. J. ELLISON, G. AHMADI and C. GRODSINSKY 1995 *Journal of Spacecraft and Rockets* **32**, 375–376. Evaluation of passive and active vibration control mechanisms in a microgravity environment.
11. N. MOSTAGHEL and J. TANBAKUCHI 1983 *Earthquake Engineering and Structural and Dynamics*, **11**, 729–748. Response of sliding structures to earthquake support motion.
12. L. SU, G. AHMADI and I. G. TADJBAKHSH 1989 *Journal of the Engineering Mechanics Division*, *ASCE* **115**, 1976–1992. A comparative study of base isolation systems.
13. F. FAN and G. AHMADI 1990 *Earthquake Engineering and Structural Dynamics* **19**, 377–388. Floor response spectra for base-isolated structures.
14. J. F. DREHER 1973 *Shock and Vibration Bulletin*, **43**, 127–139. Aircraft equipment random vibration test criteria based on vibrations induced by turbulent airflow across aircraft external surfaces.

15. R. F. HAIN, A. R. CORONADO and M. DILLARD 1993 *Air Force Flight Dynamics Laboratory*, *AFFDL-TR-93-XXX*. Bibliography of environmental data measured in flight.
16. C. P. FISHER and R. G. PRICE 1971 *General Dynamics Corporation*, *FZS*-12-321. Vibration and acoustic measurements on F-111A number 75, clean airplane in level flight.
17. J. H. WAFFORD 1979 *AGARD Report No*. 682, 1-1–1-11. Application of MIL-STD-810C dynamic requirements to USAF avionics procurements.
18. Z. GENG and L. S. HAYNES 1993 *Journal of Robotic Systems* **10**, 725–744. 6-Degree-of-freedom active vibration isolation using a Stewart platform mechanism.
19. A. HUBA 1991 *Mechatronics* **37**, 204–305. Vibration isolation of Hpt-equipment.
20. H. M. CHEN and P. LEWIS 1990 *Transactions of the ASME*, *Noise*, *Control and Acoustics* **8**, 121–124. Adaptive control for a vibration isolation mount.
21. P. G. NELSON 1991 *Review of Scientific Instruments* **62**, 2069–2075. An active vibration isolation system for inertial reference and precision measurement.
22. C. GILBERT and H. LEKUCH 1982 *Mechanical Engineering Journal* **10**, 58–63. Isolating shock and vibration.
23. M. L. TINKER and M. A. CUTCHINS 1992 *Journal of Sound and Vibration* **157**, 7–18. Damping phenomena in a wire rope vibration isolation system.
24. D. J. STECH 1993 *Journal of Guidance* **17**, 636–638. H_{2} approach for optimally tuning passive vibration absorbers to flexible structures.
25. R. HOPPE 1871 *Crelle Journal of Mathematics* **73**, 158. 1871 The bending vibrations of a circular ring.
26. L. L. PHILIPSON 1956 *Journal of Applied Mechanics* **23**, 364–366. On the role of extension in the flexural vibrations of rings.
27. S. SEIDEL and E. A. ERDELY 1964 *Journal of Engineering for Industry* **86**, 240. On the vibration of a thick ring in its own plane.
28. S. S. RAO and V. SUNDARAJAN 1969 *Journal of Applied Mechanics* **91**, 620–625. In-plane flexural vibration of circular rings.
29. S. S. RAO 1971 *Journal of Sound and Vibration* **16**, 551–566. Effects of transverse shear and rotatory inertia on the coupled twist–bending vibrations of circular rings.
30. J. KIRKHOPE 1976 *Journal of the Acoustical Society of America* **59**, 86–89. Simple frequency expression for the in-plane vibration of thick circular rings.
31. G. AHMADI and M. A. SATTER 1974 *Industrial Mathematics* **24**, 19–27. On the random vibration of a damped simply supported beam carrying concentrated masses.
32. *NASA Ames-Dryden Flight Research Facility* 1985. Process Specification No. 21-2. Environmental testing: electronic and electromechanical equipment.
33. E. C. IFEACHOR and B. W. JERVIS 1993 *Digital Signal Processing*: *A Practical Approach*. New York: Addison-Wesley Publishing Co.
34. W. SOEDEL 1993 *Vibrations of Shells and Plates*. New York: Marcel Dekker, Inc. Second edition.

APPENDIX A

Love's equations of motion governing the vibrations of a circular ring in its plane of curvature due to an applied pressure field are [34]

$$\frac{EI}{a^4}\left(\frac{\partial^2 w(\theta,\ t)}{\partial\theta^2}-\frac{\partial^3 u(\theta,\ t)}{\partial\theta^3}\right)+\frac{EA}{a^2}\left(\frac{\partial^2 w(\theta,\ t)}{\partial\theta^2}+\frac{\partial u(\theta,\ t)}{\partial\theta}\right)+q_w=M_\rho\frac{\partial^2 w(\theta,\ t)}{\partial t^2}, \quad \text{(A1)}$$

$$\frac{EI}{a^4}\left(\frac{\partial^3 w(\theta,\ t)}{\partial\theta^3}-\frac{\partial^4 u(\theta, t)}{\partial\theta^4}\right)-\frac{EA}{a^2}\left(\frac{\partial w(\theta,\ t)}{\partial\theta^2}+u(\theta,\ t)\right)+q_u=M_\rho\frac{\partial^2 u(\theta,\ t)}{\partial t^2}. \quad \text{(A2)}$$

In most applications, the extension of the neutral surface of the ring is negligible and the inextensional approximation may be used, i.e.,

$$\frac{\partial w(\theta, t)}{\partial\theta}=-u(\theta, t). \quad \text{(A3)}$$

The ring equations of motion need to be expressed in force and moment resultant form in order to apply the inextensional approximation. These equations are as follows:

$$\frac{1}{a}\frac{\partial}{\partial\theta}N_{\theta\theta}+\frac{1}{a^2}\frac{\partial}{\partial\theta}M_{\theta\theta}-M_\rho\frac{\partial^2}{\partial t^2}w(\theta,t)=-q_w, \tag{A4}$$

$$\frac{1}{a^2}\frac{\partial^2}{\partial\theta^2}M_{\theta\theta}-\frac{N_{\theta\theta}}{a}-M_\rho\frac{\partial^2}{\partial t^2}u(\theta,t)=-q_u, \tag{A5}$$

where $N_{\theta\theta}$ is the force and $M_{\theta\theta}$ is the bending moment. Solving equation (A5) for $N_{\theta\theta}$ and substituting into equation (A4) gives

$$\frac{1}{a^2}\frac{\partial^3}{\partial\theta^3}M_{\theta\theta}+\frac{1}{a^2}\frac{\partial}{\partial\theta}M_{\theta\theta}-M_\rho\frac{\partial^2}{\partial t^2}w(\theta,t)-\frac{\partial}{\partial\theta}\left[M_\rho\frac{\partial^2}{\partial t^2}u(\theta,t)\right]=-q_w-\frac{\partial q_u}{\partial\theta}. \tag{A6}$$

The resultant moment for the ring based on the tangential and normal displacements has the form

$$M_{\theta\theta}=\frac{EI}{a^2}\left(\frac{\partial}{\partial\theta}w(\theta,t)-\frac{\partial^2}{\partial\theta^2}u(\theta,t)\right). \tag{A7}$$

Using the inextensional approximation, equation (A7) can be expressed in terms of the tangential displacement as

$$M_{\theta\theta}=\frac{EI}{a^2}\left(\frac{\partial}{\partial\theta}w(\theta,t)+\frac{\partial^3}{\partial\theta^3}w(\theta,t)\right) \tag{A8}$$

or in terms of the normal displacement as

$$M_{\theta\theta}=\frac{EI}{a^2}\left(u(\theta,t)-\frac{\partial^2}{\partial\theta^2}u(\theta,t)\right). \tag{A9}$$

Substituting equations (A3) and (A8) into equation (A6) gives the equation for the tangential component of the ring motion as follows:

$$\frac{\partial^6}{\partial\theta^6}w_a(\theta,t)+2\frac{\partial^4}{\partial\theta^4}w_a(\theta,t)+\frac{\partial^2}{\partial\theta^2}w_a(\theta,t)+\frac{a^4}{EI}\frac{\partial}{\partial\theta}\left[M_\rho\frac{\partial^3}{\partial\theta\,\partial t^2}w_a(\theta,t)\right]$$
$$-\frac{M_\rho a^4}{EI}\frac{\partial^2}{\partial t^2}w_a(\theta,t)=\frac{a^4}{EI}\left(-q_w-\frac{\partial q_u}{\partial\theta}\right).$$

The normal component of the ring motion is obtained from equations (A3) and (A10).